98.10

Crystallization of Oriented Amorphous Poly(ethylene terephthalate) as revealed by X-ray diffraction and microhardness

Tsutomu Asano †, *Francisco J. Baltá Calleja, *Araceli Flores, Motonori Tanigaki, Mohammad Forhad Mina, **Chie Sawatari, **Hideyuki Itagaki, ***Hiroshi Takahashi and ***Ichiro Hatta

Department of Physics, Faculty of Science, Shizuoka University, Shizuoka 422-8529, Japan

* Instituto de Estructura de la Materia, C.S.I.C., Serrano 119, 28006 Madrid, Spain

** Faculty of Education, Shizuoka University, Shizuoka 422-8529, Japan

*** Department of Applied Physics, Graduate School of Engineering, Nagoya University, Nagoya 464-8603, Japan

† To whom correspondence should be addressed

FAX: +81-54-238-4743; E-mail:sptasan@sci.shizuoka.ac.jp

ABSTRACT

The structural changes occurring when amorphous cold-drawn poly(ethylene terephthalate) films are annealed at different temperatures (50-240°C) for different annealing times (10-10^4s) were investigated by means of X-ray diffraction and microhardness techniques. Measurements were performed at room temperature. *In-situ* X-ray scattering patterns were additionally recorded at temperatures below 100°C using synchrotron radiation. The X-ray results reveal the appearance of smectic order at 60°C with a period of 10.7Å. At 70°C, a layer structure in the scale of 110Å emerges. Finally, triclinic order is observed above 80°C. The appearance of a layer structure prior to the development of triclinic crystals is associated to a density difference along the molecular direction produced by a molecular tilting mechanism. The microhardness behaviour of annealed cold drawn PET films is correlated to the developing morphologies. At high annealing temperatures (>100°C), the plastic component of hardness is shown to vary with the occurring microstructural changes. Results indicate that the hardness of the amorphous intrafibrilar regions is higher than that of a fully amorphous material. The indentation anisotropy, ΔH, which is related to the elastic recovery of the material shows a conspicuous decrease at T_a~70°C, which is explained in terms of a relaxation of the fibrils in the chain direction.

Keywords: PET, X-ray diffraction, microhardness, layer structure, indentation anisotropy

Abbreviated title: Crystallization of Oriented Amorphous PET

INTRODUCTION

It is well known that poly(ethylene terephthalate) (PET) solidifies in the form of an amorphous glass when quenched from the melt [1,2]. Morphological studies of primary crystallization in PET were performed by several authors [3-6]. When drawing above the glass transition temperature (T_g), Bonart was the first one to report the occurrence of a paracrystalline structure [7]. This author observed that the structure of PET varied during the drawing treatment from a totally amorphous to a nematic and finally to a smectic state. From electron microscopic observations, Yeh and Geil pointed out that glassy PET is composed of ball-like structures in which molecules exhibit a paracrystalline order [8,9]. According to these authors, strain-induced crystallization can be explained by rotation, alignment and perfection of the internal order of the paracrystalline ball-like structure.

Triclinic PET sometimes reveals a unique tilted orientation (the $\bar{2}30$ orientation), which was first studied by Daubeny, Bunn and Brown [10]. Asano and Seto later analysed, in detail, the dependence of the molecular tilted orientation on the annealing temperature. These authors proposed a monoclinic paracrystalline structure in the early stages of crystallization from an oriented glass [11] which enables to explain the variation of the tilted orientation.

Microindentation studies on a wide variety of polymeric materials provide experimental evidence of a close relationship between microhardness and several microstructural parameters such as the crystalline lamellar thickness, crystallinity, polymorphism, etc. [12-14]. Microhardness of isotropic PET has been extensively studied [15-18]. Santa Cruz *et al.* [15] measured *in-situ* the variation of H with crystallization time at a crystallization temperature, T_a, of 117°C. During primary crystallization, H was shown to linearly rise with the increasing volume fraction of spherulites, from H_a~120 MPa

(amorphous material) up to H~200 MPa (fully spherulitic material). In samples in which the spherulitic growth is complete ($T_a \geq 120°C$), hardness was shown to be nearly constant with increasing annealing temperature. The microhardness of injection-moulded PET at different mould temperatures has also been investigated [16]. Hardness values measured on the outer surface and in the centre of the mouldings were shown to vary with the mould temperature according to the developing morphology. The crystallization kinetics from the glassy state has also been studied on isotropic PET by microindentation hardness for different crystallization temperatures [17]. The microhardness of melt crystallized PET samples under high pressure (~4kbar) has been recently reported [18]. Unprecedentedly high hardness values were found (H=300-400 MPa) due to unusual high crystallinity and high crystalline lamellar thickness values. Furthermore, the mechanical anisotropy of injection moulded PET has been recently measured [19].

In the present paper, we report new morphological studies of cold drawn PET as revealed by X-ray diffraction and hardness measurements. The mechanism of crystallization of oriented glassy PET, especially in the initial stages of crystallization below 100°C, is discussed. The correlation between the structure developed during crystallization of drawn PET and the corresponding mechanical properties is highlighted.

EXPERIMENTAL

Cold drawing and annealing treatments

Amorphous PET was synthesized by Toray Co. Ltd. Japan (M_n=18,000). The isotropic sample film (thickness ~0.5mm) was drawn at room temperature using a Tensilon UTM 4-100, Toyo Boldwin Co. Ltd. The drawing speed and the average draw ratio were 0.8mm/min and 3.8, respectively. The film was slightly whitened by the uniaxial drawing, with final thickness of 0.15mm.

The annealing treatment of the cold drawn PET samples was performed with fixed ends maintaining the length of the sample constant. Samples annealed at temperatures, T_a, lower than 160°C were immersed in a silicone oil bath. The temperature is controlled with an accuracy of ±0.1°C. The annealing times, t_a, used for each annealing temperature were 10, 10^2 and 10^3s. An oven was used to anneal the samples above 160°C. Due to the low heat conductivity of the air oven, only long annealing times were used. Hence, samples annealed at temperatures in the range 50-240°C for 10^4s were prepared.

X-ray diffraction measurements

Wide angle (WAXS), middle angle (MAXS) and small angle (SAXS) X-ray scattering patterns of the annealed samples were obtained. MAXS experiments were carried out in order to simultaneously record the WAXS and SAXS diffraction maxima in one photograph (2θ ~1-10°).

WAXS and SAXS patterns of the annealed samples were taken at room temperature using a Rigaku 4012A and RU300 generator, respectively, with a wavelength of 1.54Å. The camera length and exposure time were 5cm and 1hr for the WAXS experiments and 26cm and 3hrs for the SAXS measurements. The WAXS patterns recorded correspond to the samples annealed at $T_a \leq 100$°C (t_a=10-10^4s). SAXS experiments were carried out on samples annealed at $T_a \geq 100$°C for t_a=10^4s.

In-situ MAXS measurements were performed at Photon Factory, National Laboratory for High Energy Physics, Tsukuba, Japan, using a vacuum path with a camera length of 86cm. The oriented amorphous sample was sandwiched between two metal rings of 7mm in diameter to prevent shrinkage during heating. The metal rings were then placed in the Mettler FP-99 heating facility [20]. The sample was heated at 10°C/min up to T_a ($T_a \leq 100$°C) and held thereafter for 60s. The exposure time for one MAXS pattern

photographed by Imaging Plate (IP) of Fuji Film Co. Ltd. was 60s. The wavelength used was 1.506 Å.

Density

The density, ρ, of the drawn PET samples annealed at different temperatures for 10^4s was measured by the floating method using a Lipkin's pycnometer, with n-heptane and carbon tetrachloride as a medium.

Degree of crystallinity

The volume degree of crystallinity, α_c, of the investigated PET samples was derived from density following:

$$\alpha_c=(\rho-\rho_a)/(\rho_c-\rho_a) \quad (1)$$

where ρ_a and ρ_c are the densities of the amorphous and crystalline phases respectively. The amorphous density of PET is taken to be ρ_a=1.37 g/cm^3, which is the measured density of the amorphous cold drawn sample without further annealing (see below). The density of the triclinic crystalline phase of PET is taken to be [10] ρ_c=1.455 g/cm^3.

Microhardness

Microindentation experiments were carried out at room temperature (~21°C). A Vickers square-based diamond pyramid (included angle between opposite faces 2α=136°) was used. Vickers hardness is calculated following:

$$H = k\frac{P}{d^2} \quad (2)$$

where P is the load applied, d the measured diagonal of the residual impression and k is a geometric constant. A value of k=1.854 is used when P is in N and d in mm to give H in MPa. The load applied was of 980 mN, which was held for six seconds to minimize the creep of the sample under the indenter [12]. The P/d^2 ratio was observed to be constant for different loads, i. e. the elastic recovery was negligible [21]. The accuracy in the indentation

diagonal was of ±1.2μm. Due to sample orientation, the residual impression shows anisometric diagonal lengths. We define $H_{\parallel}$ as the hardness derived from the measurement of the indentation diagonal parallel to the drawing direction and $H_{\perp}$ as the value derived from the diagonal length perpendicular to the drawing direction. The indentation anisotropy, ΔH, is calculated following [12]:

$$\Delta H\,(\%) = 1 - \frac{H_{\perp}}{H_{\parallel}} \tag{3}$$

Mechanical models

The hardness of a polymeric material, H, is well described by a parallel model of alternating amorphous and crystalline regions, with hardness values H_a and H_c respectively, following [13]:

$$H = H_c\,\alpha_c + H_a\,(1-\alpha_c) \tag{4}$$

where α_c is the volume degree of crystallinity. H_c is related to the crystalline lamellar thickness, l_c, through [13]:

$$H_c = \frac{H_c^{\infty}}{1 + \frac{b}{l_c}} \tag{5}$$

where H_c^{∞} is the hardness of an infinitely thick crystal and $b=2\sigma_e/\Delta h$ is a parameter related to the surface free energy σ_e of the crystals and to the energy Δh required for plastic deformation of the latter.

RESULTS

Measurements at room temperature

Wide angle X-ray scattering (WAXS)

The WAXS patterns of cold drawn PET annealed at different temperatures (t_a=10s) are presented in *Figure 1*. X-ray diffraction of the original cold-drawn sample has a broad maximum centred on the equator. The scattering pattern does not change upon annealing at 50°C for 10s (*Figure 1a*). The occurrence of a diffuse equatorial diffraction maximum indicates that PET molecules are preferentially aligned parallel to the draw direction with absence of crystalline order.

In *Figures 1b-1d*, a weak but sharp reflection appears on the meridian. The spacing of this reflection is measured as 10.7Å. We index this reflection as 001' since the spacing nearly corresponds to the monomer length (10.75 Å) of PET. The 001' reflection also appears when the amorphous sample is annealed at 50°C for 10^2s. The intensity of the 001' reflection changes in the temperature range of 60-80°C, depending on T_a and t_a. The highest intensity of 001' for t_a=10s is observed at T_a=70°C, as shown in *Figure 1c*. The equatorial maximum is still rather broad below 70°C indicating that the oriented PET molecules have no lateral crystalline order. For T_a>80°C, the intensity of the 001' reflection clearly decreases. Simultaneously, the triclinic 010 and $0\bar{1}1$ reflections become distinct from the equatorial diffuse peak. At T_a=90°C, the meridional 001' reflection almost disappears and the equatorial triclinic 010 reflection increases in intensity (see *Figure 1e*). At T_a=100°C, the triclinic 010 reflections are displaced up and down from the equator, indicating that the triclinic (010) plane is inclined by 10° from the draw-direction (see *Figure 1f*).

Small angle X-ray scattering (SAXS)

SAXS measurements on samples annealed at $T_a \geq 100°C$ for $t_a = 10^4$s yield four-point patterns (see *Figure 2* for $T_a = 220°C$). From the 4-point patterns recorded, we can evaluate the lamellar spacing, L, along the drawing direction and the lamellar inclination angle, ϕ, between the normal to the lamellar and the drawing direction. The values of L and ϕ for different T_a are listed in Table I.

Density

Figure 3 illustrates the plot of the density of the drawn samples vs. T_a ($t_a = 10^4$s). The density of the oriented glassy PET sample ($T_a = 20°C$) is 1.37g/cm^3, i.e. higher than the value of isotropic amorphous PET (1.335g/cm^3)[10]. The density values show a monotonous increase with T_a. The crystalline lamellar thickness along the axis normal to the lamella, l_c, was evaluated from:

$$l_c = \alpha_c \, L \cos\phi \qquad (6)$$

where α_c is derived from density measurements using equation (1). The values of α_c and l_c for $T_a \geq 100°C$ are also listed in Table I.

Microhardness

Figure 4 shows $H_\parallel$ and $H_\perp$ values as a function of the annealing temperature for different annealing times. The hardness value for the cold drawn sample before annealing ($T_a = 20°C$) has also been included. $H_\perp$ values are related to the plastic deformation mode of the lamellar stacks within the fibrous oriented structure. The higher $H_\parallel$ values with respect to the $H_\perp$ values for the four series of annealed PET samples ($t_a = 10, 10^2, 10^3$ and 10^4s) are a consequence of the instant elastic recovery of the fibrils after removal of the indenter and therefore contribute to the smaller indentation dimension.

Figure 5 illustrates the variation of the indentation anisotropy as a function of T_a for the series of PET samples annealed at different t_a. Anisotropy ΔH is a measure of the

elastic recovery of the material and has been correlated to the longitudinal elastic modulus in other oriented polymer samples [12, 22]. The first finding in *Figure 5* is the unusual high ΔH values found for the samples investigated. At the lowest annealing temperatures (T_a < 70°C), ΔH~40%, which is a large indentation anisotropy value as compared to that reported on injection moulded PET [19] where the maximum ΔH achieved was of 15%. Most interesting is the fact that above T_a~70°C, which is a temperature close to the glass transition temperature (T_g) of PET, ΔH decreases rapidly with T_a.

***In-situ* MAXS measurements**

The results of the MAXS experiments are shown in *Figure 6*. The isotropic rings in the MAXS patterns are artifacts originated from the polymer film placed in the vacuum path. The meridional 001' reflection is located out of the isotropic ring as indicated in *Figure 6c*. The SAXS reflection appears near the centre of the pattern at temperatures 70°C and above (*Figures 6c-6f*). The spacing of the SAXS reflection is approximately constant over the range of T_a considered and equal to 110Å. Hence, the lamellar along the drawing direction comprises roughly 10 monomer units. The inclination angle ϕ at T_a=70°C is ~62°. As the annealing temperature increases, the meridional reflection progressively weakens while the SAXS reflection increases in intensity. At T_a=100°C, the meridional 001' reflection has completely disappeared.

DISCUSSION

Crystallization process

In order to summarize the various steps of the crystallization process from the glass, the results of the WAXS, MAXS and SAXS measurements are schematically illustrated in *Figure 7*. The intensity of the meridional, the SAXS and the triclinic reflection at different temperatures are compared in Table II .

Molecular orientation by cold drawing

Cold drawing of glassy PET at room temperature through necking induces preferential alignment of the chain axis along the draw-direction. Some molecular segments could be randomly oriented or partly entangled due to the limited mobility at temperatures well below T_g. However, considering the applied draw-ratio of 3.8 and the high density achieved (1.37 g/cm^3), one must conclude that a significant number of molecules are aligned nearly parallel to the draw-direction. The orientational order exhibited could be described by a nematic state as schematically depicted in *Figure 8a*. The circles in the molecular chains represent benzene rings separated by 10.75Å intervals. The lateral position of each benzene ring deviates with respect to the neighbouring molecules.

Analysis of the meridional reflection

The meridional reflection is first apparent at T_a=50-60°C (depending on t_a). The spacing is almost equal to the monomer unit length. This result suggests that neighbouring molecular segments laterally tend to match at temperatures below T_g.

Figure 8b schematically shows the occurrence of the smectic phase developed from the nematic state. The benzene rings of the smectic state are arranged on planes perpendicular to the draw direction, whereas the lateral packing of the neighbouring molecules has no crystalline order. The smectic state is presumably attained through an increase in the mobility of the molecular segments leading to a slightly higher densely packed structure (ρ=1.38 g/cm^3) than that of the nematic one.

Development of the lamellar structure

The appearance of a diffuse SAXS reflection (long range order) at T_a=70°C prior to the development of the triclinic crystal (short range order) is most interesting. The result suggests the existence of a precursor state before the triclinic state. Considering that here T_a is on the vicinity of T_g, molecular motions are insufficient so as to form a long range

order. Hence, we propose a molecular tilting mechanism in the smectic phase which implies a minimum cooperative displacement. This tilting mechanism could produce a density difference within the smectic structure and hence could explain the long range order observed in MAXS. The precursor state at T_a=70°C is schematically illustrated in *Figure 9*.

Tilting mechanism

One possibility to explain the periodic density difference observed along the molecular direction at T_a=70°C could be in terms of a combination of a molecular tilt mechanism and the inclination of the layer surface. To estimate the density difference along the molecular direction, we first calculate the average lateral distance between molecules in the smectic state. The volume of the triclinic unit cell, V_c, from ref. 10 is 218.95Å^3. The average smectic volume, V_{sm}, is estimated as follows:

$$V_{sm} = (\rho_c/\rho_{sm})V_c = 230.85\text{Å}^3 \quad (7)$$

where ρ_c=1.455g/cm^3 [10] and ρ_{sm}=1.38g/cm^3 is the smectic density observed at 70°C (see *Figure 3*). The average molecular cross section is derived as 230.85Å^3/10.75Å=21.47Å^2 and the average molecular distance is calculated as 5.23Å (see *Figure 9a*).

If we assume that the lamellar surface fits to the shift of one monomer unit (see *Figure 9a*), then the inclination angle of the lamellar ϕ is calculated as:

$$\phi = \tan^{-1}(10.75/5.23) = 64° \quad (8)$$

This value is consistent with the value (~62°) obtained from the MAXS pattern at 70°C.

Assuming that the tilt of the smectic molecules alternates by an angle $\pm\delta$ from the draw-direction, the inclined layer produces a packing difference between regions A and C (*Figure 9a*). The ratio between the densities in the A and C regions can be calculated from the ratio between the lateral dimensions in A and C, d_A/d_C. For a value of δ=1°:

$$d_A/d_C = \sin(90°-64°+\delta)/\sin(90°-64°-\delta) = 1.074 \quad (9)$$

On the other hand, the quotient between the amorphous and the triclinic density is equal to:

$$\rho_c/\rho_a = 1.455/1.37=1.062 \quad (10)$$

Thus the estimated d_A/d_C ratio in the precursor state seems to be sufficient to produce the required electron density contrast. Moreover, using δ=1° and L=110Å, the maximum lateral deviation, Δx, from the draw-direction is calculated to be less than 1Å (*Figure 9b*). The small δ and Δx values are likely to occur on the initial stages of crystallization at temperatures on the vicinity of T_g.

The above discussion strongly suggests that a tilting mechanism could produce the precursor state at 70°C.

Development of triclinic crystals

The WAXS results in *Figure 1* indicate that the triclinic crystal develops above 80°C. In the preceding section, we suggest that the precursor state is formed by a slight tilt of the smectic molecules. The triclinic structure is then developed at T_a>80°C by a further tilt of the molecules within the crystalline lamellae. As shown in the WAXS patterns of *Figure 1f*, the triclinic (010) plane is 10° inclined from the draw-direction. Considering the triclinic crystal structure with the crystallographic angle α=98.5° [10], the crystalline b-axis is nearly perpendicular to the draw-direction. This fact strongly supports the concept that the normal to the benzene rings' planes is maintained parallel to the draw-direction during the initial crystallization process from the smectic structure through the precursor state into the triclinic phase. *Figure 8c* schematically shows the development of the triclinic crystals at 100°C with the b-axis nearly perpendicular to the draw-direction.

Further annealing at higher temperatures thickens the crystalline lamellae as shown in Table I. Entanglements and folds will concentrate especially at high T_a, in the amorphous lamellae.

Mechanical properties: microhardness

Influence of annealing temperature

In *Figure 4*, one can distinguish four regions of $H_\perp$ behaviour which correlate to the various structures appearing when T_a is increased:

i) $T_a \leq 60°C$. WAXS diagrams reveal the existence of an amorphous oriented phase at room temperature and the emerging of a smectic order at T_a = 50-60°C (see *Figure 1b*). These structural changes occurring below 60°C do not seem to substantially influence the $H_\perp$ values.

ii) $60°C < T_a \leq 80°C$. In this temperature range, $H_\perp$ slightly varies with T_a. Here the smectic phase is the main structure appearing. At T_a= 70°C, the amount of smectic domains present is sufficient to produce an appreciable $H_\perp$ increase. In addition, a layer structure emerges at T_a= 70°C as revealed by MAXS (see *Figure 6c*).

iii) $80°C < T_a < 100°C$. The $H_\perp$ increase observed above 70° C can be considered as due to an enhancement of molecular motion facilitated beyond T_g. The steep $H_\perp$ variation with T_a from T_a = 80°C up to T_a ~ 100°C is associated to the developing of a triclinic structure while the smectic domains start to disappear.

iv) $T_a \geq 100°C$. At T_a=100°C, the smectic phase has completely disappeared and a three-dimensional crystalline order has developed as revealed by WAXS (see *Figure 1*). Contrary to what was observed for isotropic PET [15], there is a further hardness increase with T_a (>100°C) up to the highest annealing temperature. This $H_\perp$ increase could be related to the structural changes occurring in the fibrils as will be discussed below.

Influence of annealing time

From *Figure 4* one observes a tendency of $H_\perp$ to increase with increasing annealing time. The hardness increase with t_a for 50°C < T_a < 80°C could be related to a densification of

the amorphous phase and/or an increase in the number or perfection of the smectic domains. For samples in which the triclinic structure is apparent ($T_a > 80°C$), the higher $H_\perp$ values observed at long annealing times could be also related to an increase in crystallinity and crystalline lamellar thickness with t_a.

Elastic recovery

The rapid indentation anisotropy decrease for T_a~70°C (see *Figure 5*) is connected with the concurrent decrease in the elastic properties of the fibrils which most probably relax with increasing annealing temperature. It has been shown that after a change from nematic (20°C) to smectic (60°C), the precursor state appears at 70°C and the triclinic structure develops above 80°C. The indentation anisotropy decrease could be related to the development of the lamellar structure starting at about 70°C. One may imagine that in the amorphous layers, the local molecular orientation will be influenced by the relaxation mechanism occurring above T_g. As a result, the elastic recovery in chain direction will decrease with increasing concentration of relaxed molecules in the amorphous layers. The observed decrease in the angle of lamellar inclination (ϕ) as T_a increases is in accordance with the suggested relaxation of the molecules in the amorphous layers. In spite of that, it is interesting to note that a rest of the mechanical anisotropy still remains preserved up to temperatures near the melting point.

Influence of the crystallinity

Hardness is known to vary with α_c following equation (4). The α_c values as derived from equation (1), continuously increase with T_a analogously to the ρ variation with T_a shown in *Figure 3*. However, for $T_a < 100°C$, the α_c increase is mainly due to the densification of smectic domains. Hence, the $H_\perp$ increase up to T_a=100°C in *Figure 4* is mainly due to an increase of ρ rather than to the occurrence of X-ray crystallinity. Previous studies on isotropic semicrystalline PE had shown that H conspicuously varies with the macroscopic

density [23, 24]. The $H_\perp$ variation with T_a for $T_a \geq 100°C$ could be partly due to the α_c-increase with increasing annealing temperature (see equation (4)). Additionally, the microstructural changes occurring when raising the annealing temperature also contribute to a $H_\perp$ increase (see below).

Hardness-microstructure correlation

According to equation (4), the hardness should linearly increase with α_c. On the other hand, H_c is known to vary with l_c according to equation (5). We have seen that the crystallinity and crystal thickness increase with T_a (Table I). In order to evaluate the independent influence of α_c and l_c on hardness, we have represented in *Figure 10* the variation of $H_\perp$ vs. α_c. The $H_\perp$ values for $T_a<100°C$ have been included and the corresponding α_c-values should be interpreted as discussed above. Equation (4) could now be rewritten as:

$$H_\perp = \alpha ((H_c)_\perp - (H_a)_\perp) + (H_a)_\perp \qquad (11)$$

Each $H_\perp$ value (for $T_a \geq 100°C$) in *Figure 10* fits to a straight line with slope $(H_c)_\perp - (H_a)_\perp$ and intercept $(H_a)_\perp$. If $(H_a)_\perp$ is known, then $(H_c)_\perp$ can be derived for each sample and subsequently related to the corresponding l_c value. If we approximate the $(H_a)_\perp$ value to the hardness of the cold drawn sample ($\alpha_c=0$, $(H_a^{glass})_\perp$ = 75 MPa), then one would obtain a $(H_c)_\perp$ value (independent of l_c) of about 325 MPa for the samples annealed at $T_a \geq 140°C$ ($\alpha_c \geq 0.35$). Indentation experiments on PET microfibrils, which show a very high degree of crystallinity ($\alpha_c \sim 1$) and nearly extended chains ($l_c \rightarrow \infty$) , give an $H_\perp$ value of 360 MPa [25]. Thus, not only the obtained value of $(H_c)_\perp^\infty \sim 325$ MPa seems rather low but makes also difficult to explain why our $(H_c)_\perp$ values do not vary with increasing l_c. This result suggests that the hardness of the amorphous constrained regions within the crystals should be higher than that of a completely amorphous oriented sample. On the other hand, the upper limit to the $(H_a)_\perp$ value is 140 MPa, which is the hardness of the sample annealed at $T_a=100°C$

(α_c=0.22), where the smectic domains have completely disappeared (see *Figure 1f*). If we assume a value of $(H_a)_\perp$=140 MPa, we may draw a family of straight lines (see equation (11)), which are included in *Figure 10*. Extrapolation of equation (11) at α_c=1 gives the crystal hardness $(H_c)_\perp$ for each l_c value. The same procedure could be applied for $(H_a)_\perp$ values in the range 75-140 MPa. Next section discusses the most reasonable $(H_a)_\perp$ values for the amorphous constrained phase based on the analysis of the $(H_c)_\perp$ vs. l_c data.

Hardness of infinitely thick crystals

According to equation (5), a plot of $1/(H_c)_\perp$ values versus $1/l_c$ values will fit into a straight line (if b is constant) of slope $b/(H_c^\infty)_\perp$ and ordinate intercept $1/(H_c^\infty)_\perp$. *Figure 11* illustrates the variation of $1/(H_c)_\perp$ with $1/l_c$ for samples annealed at $T_a \geq 180°C$ ($\alpha_c \geq 0.5$). In the derivation of the $(H_c)_\perp$ values, a value of $(H_a)_\perp$ =140 MPa was used. The data in *Figure 11* fit to a straight line. The intercept gives $(H_c^\infty)_\perp$=358 MPa, which is in excellent agreement with $H_\perp$ of highly crystalline chain-extended PET microfibrils (=360 MPa) [25]. Lower $(H_a)_\perp$ values would yield higher intercepts and hence, smaller $(H_c^\infty)_\perp$ values. The above analysis suggests that the hardness value for the amorphous constrained regions ($(H_a)_\perp$ ~140MPa) is higher than that of the starting oriented amorphous material.

CONCLUSIONS

1) The sharp reflection on the meridian corresponding to a period of 10.7Å, induced after annealing cold drawn PET at 60°C, has been associated to the occurrence of a smectic structure.
2) The SAXS maxima observed at 70°C indicate that a density fluctuation of 110Å appears as a precursor before triclinic crystallisation. From the SAXS pattern it is inferred that the layer structure is initially inclined about 62° from the draw-direction.

3) Triclinic crystallisation starts above 80°C, where the (010) planes are inclined by 10° from the draw-direction.

4) The crystallization mechanism from the smectic structure, via the precursor state, into the final triclinic crystal is explained by a tilting mechanism. The molecular tilt and the inclination of the lamellar surface produce a density difference between regions in the precursor state. The triclinic crystals develop by a further tilt of 10°.

5) The hardness measurement of annealed oriented PET films permits to distinguish between: a) amorphous oriented samples, b) the smectic phase and c) the crystalline fibrils.

6) Indentation anisotropy (related to elastic recovery) conspicuously decreases above T_a~70°C (i.e. near T_g). This has been ascribed to a relaxation mechanism of the molecules in the amorphous layers in the chain direction.

7) Results suggest that the hardness value of the amorphous constrained regions within the semicrystalline fibrils is higher than that of the starting amorphous oriented material.

ACKNOWLEDGEMENTS

Grateful acknowledgement is due to the Dirección General de Investigación Científica y Técnica (DGICYT), Spain, for support of this investigation (Grant PB94-0049). A part of this work has been performed under approval of the Photon Factory Advisory Committee (Proposal No. 97G248).

REFERENCES

1. Keller, A., Lester, G. R., Morgan, L. B., Hartley, F. D. and Lord, E. W. *Phil. Trans. R. Soc.* A-1 1954, **247**, 13

2. Zachmann, H. G. and Stuart, H. A. *Makromol. Chem.* 1960, **41**, 131

3. Elsner, G., Koch, M. H. J., Bordas, J. and Zachmann, H. G. *Makromol. Chem.* 1981, **181**, 1263

4. Elsner, G., Rickel, C. and Zachmann, H. G. *Adv. Polym. Sci.* 1985, **67**, 1

5. Günter, B. and Zachmann, H. G. *Polymer* 1983, **24**, 1008

6. Asano, T., Zdeick-Pickuth, A. and Zachmann, H. G. *J. Mater. Sci.* 1989, **24**, 1967

7. Bonart, R. *Kolloid-Z.* 1966, **213**, 1

8. Yeh, G. S. Y. and Geil, P. H. *J. Macromol. Sci.* B 1967, **1**, 235

9. Yeh, G. S. Y. and Geil, P. H. *J. Macromol. Sci.* B 1967, **1**, 251

10. Daubeny R. de P., Bunn, C. W. and Brown, C. J. *Proc. Roy. Soc., A* 1954, **226**, 531

11. Asano T. and Seto T. *Polym. J.* 1973, **5**, 72

12. Baltá Calleja, F. J. *Adv. Polym. Sci.* 1985, **66**, 117

13. Baltá Calleja, F. J. *Trends Polym. Sci.* 1994, **2**, 419

14. Baltá Calleja, F. J. and Fakirov, S. *Trends Polym. Sci.* 1997, **5**, 246

15. Santa Cruz, C., Baltá Calleja, F. J., Zachmann, H. G., Stribeck, N. and Asano, T. *J. Polym. Sci., Polym. Phys., B* 1991, **29**, 819

16. Baltá Calleja, F. J., Baranowska, J., Rueda, D. R. and Bayer, R. K. *J. Mater. Sci.* 1993, **28**, 6074

17. Baltá Calleja, F. J., Santa Cruz, C. and Asano, T. *J. Polym. Sci., Polym. Phys., B* 1993, **31**, 557

18. Baltá Calleja, F. J., Öhm, O. and Bayer, R. K. *Polymer* 1994, **35**, 4775

19. Rueda, D. R., Kubera, L., Baltá Calleja, F. J. and Bayer, R. K. *J. Mater. Sci. Lett.* 1993, **12**, 1140

20. Hatta, I., Takahashi, H., Matuoka, S. and Amemiya, Y. Therm. Acta 1995, **253**, 149

21. Baltá Calleja, F. J., Rueda, D. R., Porter, R. S. and Mead, W. T. *J. Mater. Sci.* 1980, **15**, 765

22. Rueda, D. R., Baltá Calleja, F. J., García Peña, J., Ward, I. M. and Richardson, A. *J. Mater. Sci.* 1984, **19**, 2615

23. Baltá Calleja, F. J., Martínez Salazar, J. Cackovic, H. and Loboda-Cackovic, J. *J. Mater. Sci.* 1981, **16**, 739

24. Martínez Salazar, J. and Baltá Calleja, F. J. *J. Mater. Sci.* 1983, **18**, 1077

25. Krumova, M., Fakirov, S., Baltá Calleja, F. J. and Evstatiev, M. *J. Mater. Sci.* 1998, **33**, 000

T_a (°C)	L (Å)	ϕ (°)	α_c	l_c (Å)
100	110	55	0.22	14
120	111	50	0.28	20
140	113	46	0.35	28
160	117	44	0.41	35
180	120	41	0.48	44
200	124	40	0.55	52
220	140	38	0.63	70
240	158	37	0.72	91

Table I. Long period in the drawing direction, lamellar inclination angle, degree of crystallinity and crystalline lamellar thickness for PET annealed at a temperature T_a (t_a=10^4s).

T_a (°C)	001' (WAXS)	Triclinic (WAXS)	Layer (SAXS)
Room temp.	×	×	×
50	Δ	×	×
60	o	×	×
70	o	×	Δ
80	o	Δ	o
90	Δ	o	o
100	×	o	o

Table II. Observation of 001', triclinic reflections in WAXS and layer structures in SAXS.

×: disappearance Δ: weak appearance o: appearance

CAPTIONS TO FIGURES

Figure 1. WAXS patterns of cold drawn PET taken at room temperature after annealing during 10s at a temperature of: a) 50°C, b) 60°C, c) 70°C, d) 80°C, e) 90°C and f) 100°C.

Figure 2. SAXS diagram of the PET film annealed at 220°C for $t_a = 10^4$s.

Figure 3. Density variation with annealing temperature ($t_a=10^4$s).

Figure 4. $H_{\parallel}$ and $H_{\perp}$ as a function of the annealing temperature for different annealing times: ∇: $t_a = 10$ s; ◊: $t_a = 10^2$ s; Δ: $t_a = 10^3$ s; O: $t_a = 10^4$ s; ▼: cold drawn sample without further annealing.

Figure 5. ΔH as a function of the annealing temperature for different annealing times. Symbols as in *Figure 4.*

Figure 6. In-situ MAXS patterns obtained at different annealing temperatures: a) 50°C, b) 60°C, c) 70°C, d) 80°C, e) 90°C, f) 100°C.

Figure 7. Summary of the X-ray results during the crystallization.

Figure 8. Schematic representation of the morphological changes: a) nematic phase, b) smectic phase and c) triclinic structure.

Figure 9. The tilting mechanism occurring in the precursor state. (a) The density difference between A and C regions. (b) The molecular displacement in the precursor state.

Figure 10. $H_{\perp}$ variation with α for the samples annealed during 10^4s. The straight lines follow equation (4), with $(H_a)_{\perp}$=140 MPa.

Figure 11. Plot of $(H_c)_{\perp}^{-1}$ as a function of l_c^{-1}. Open circle: $H_{\perp}$ of highly crystalline chain-extended PET microfibrils.

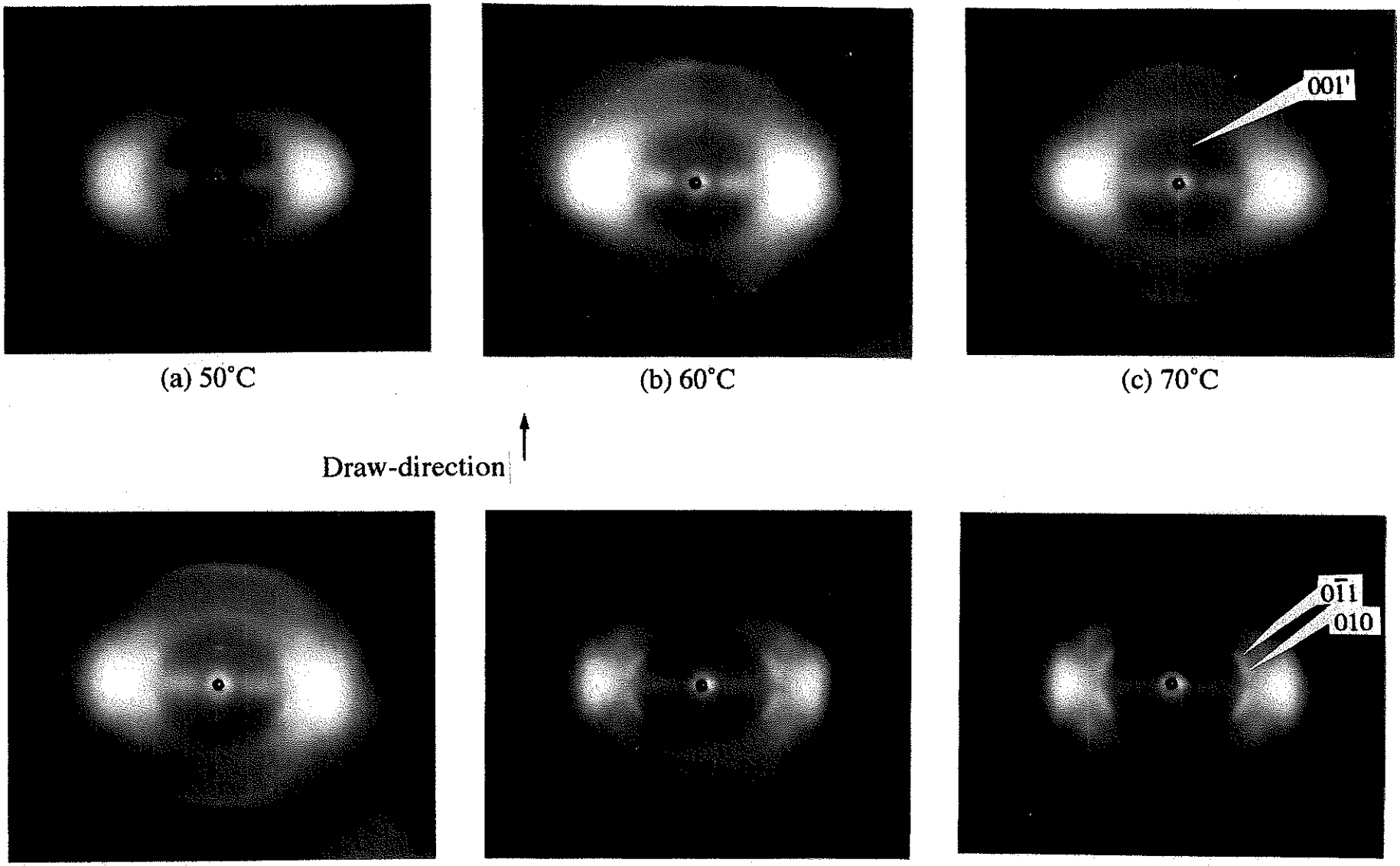

(a) 50°C (b) 60°C (c) 70°C

(d) 80°C (e) 90°C (f) 100°C

Fig. 1

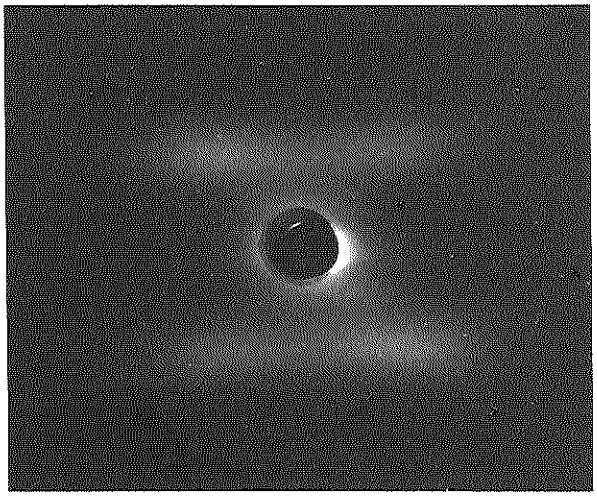

Fig. 2

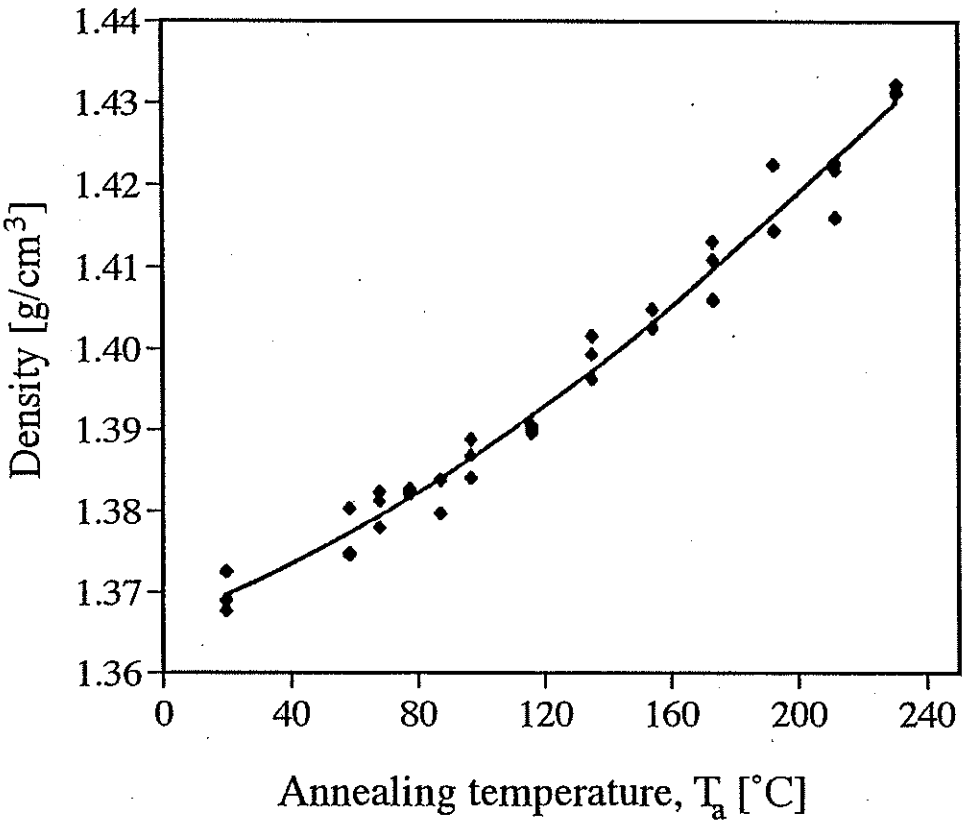
1.44
1.43
1.42
1.41
1.40
1.39
1.38
1.37
1.36
Density [g/cm^3]
0
40
80
120
160
200
240
Annealing temperature, T_a [°C]

Fig.3

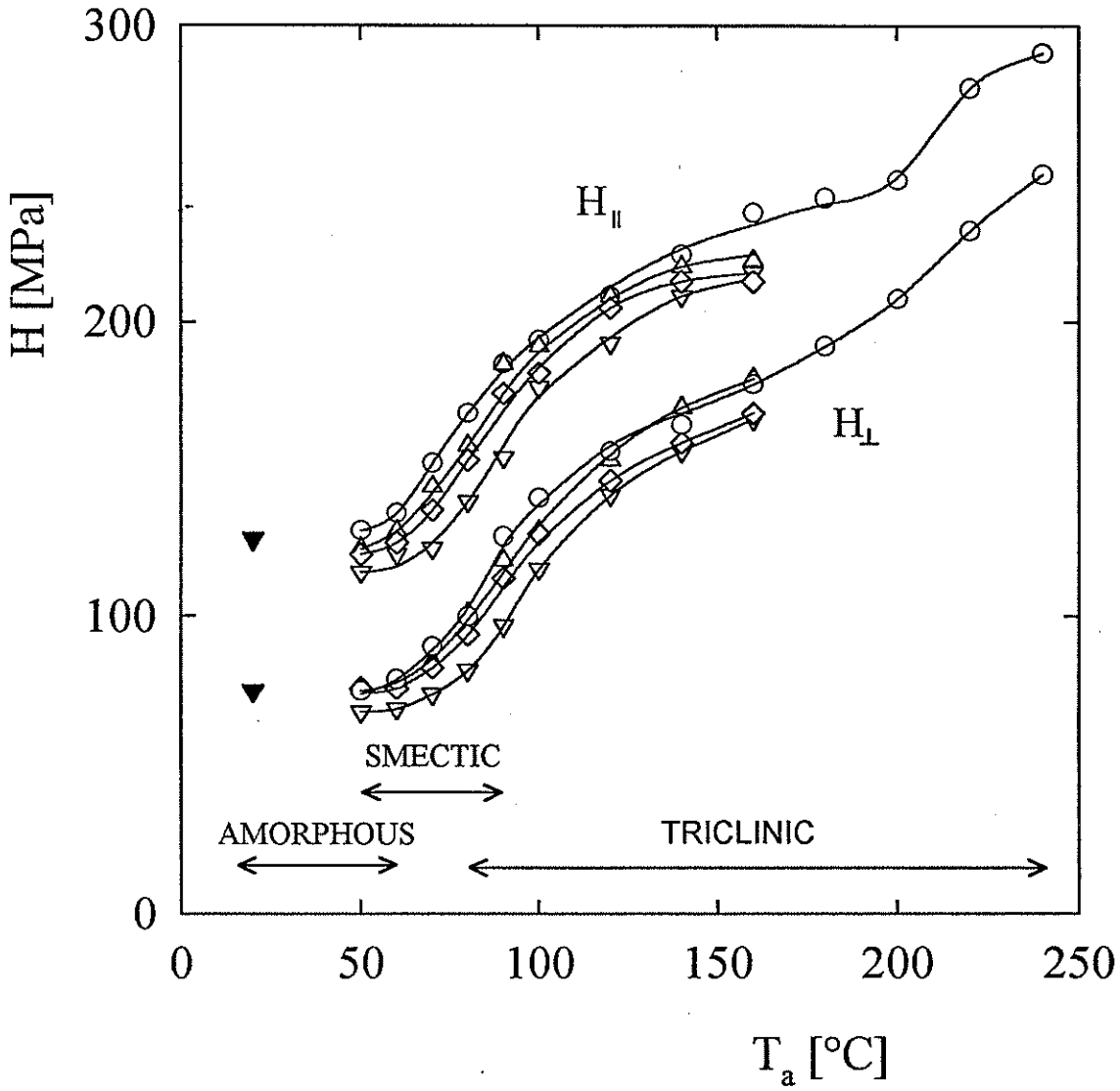
300
200
100
0
H [MPa]
$H_{\parallel}$
$H_{\perp}$
SMECTIC
AMORPHOUS
TRICLINIC
0
50
100
150
200
250
T_a [°C]

Fig. 4

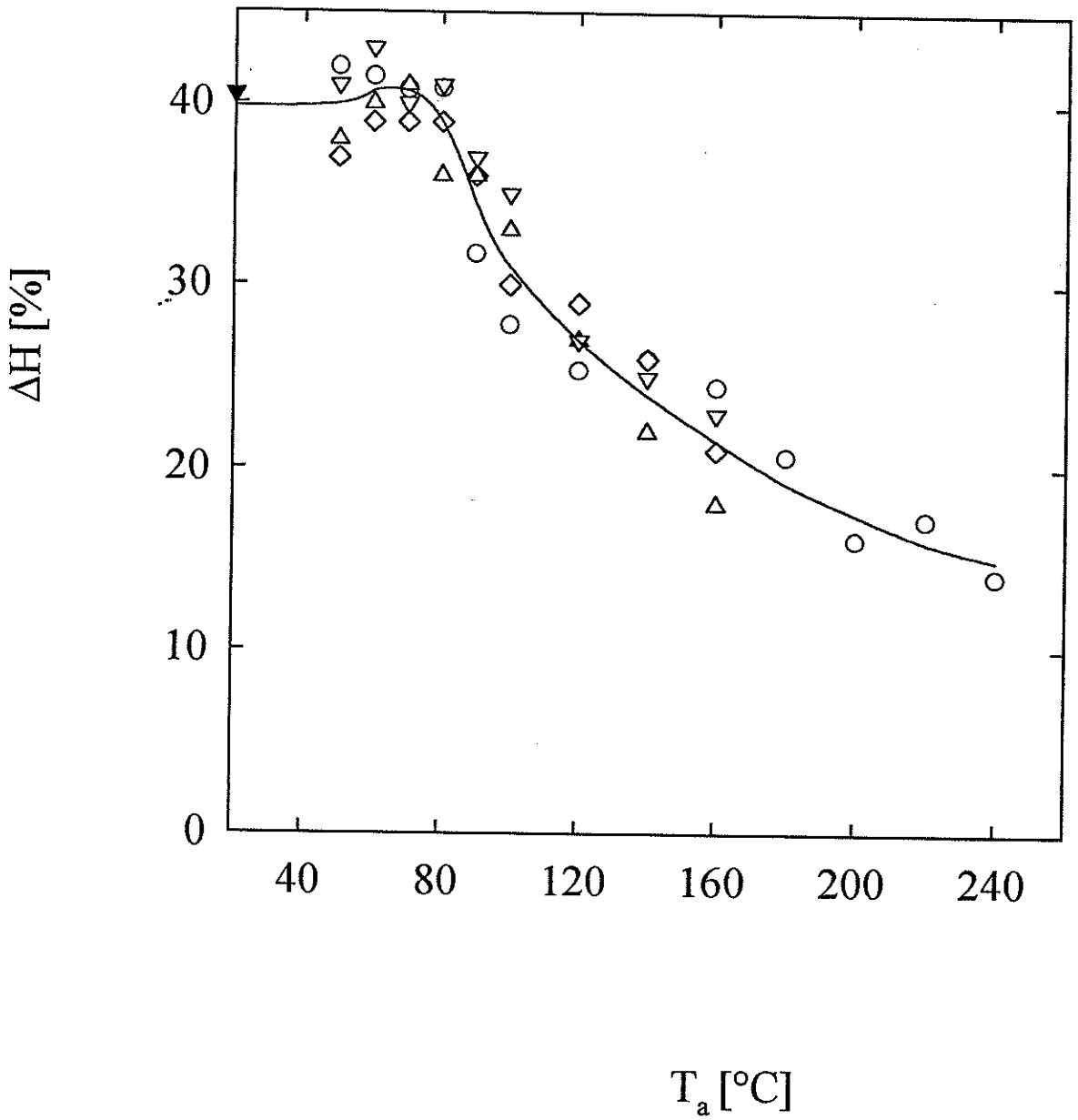

Fig. 5

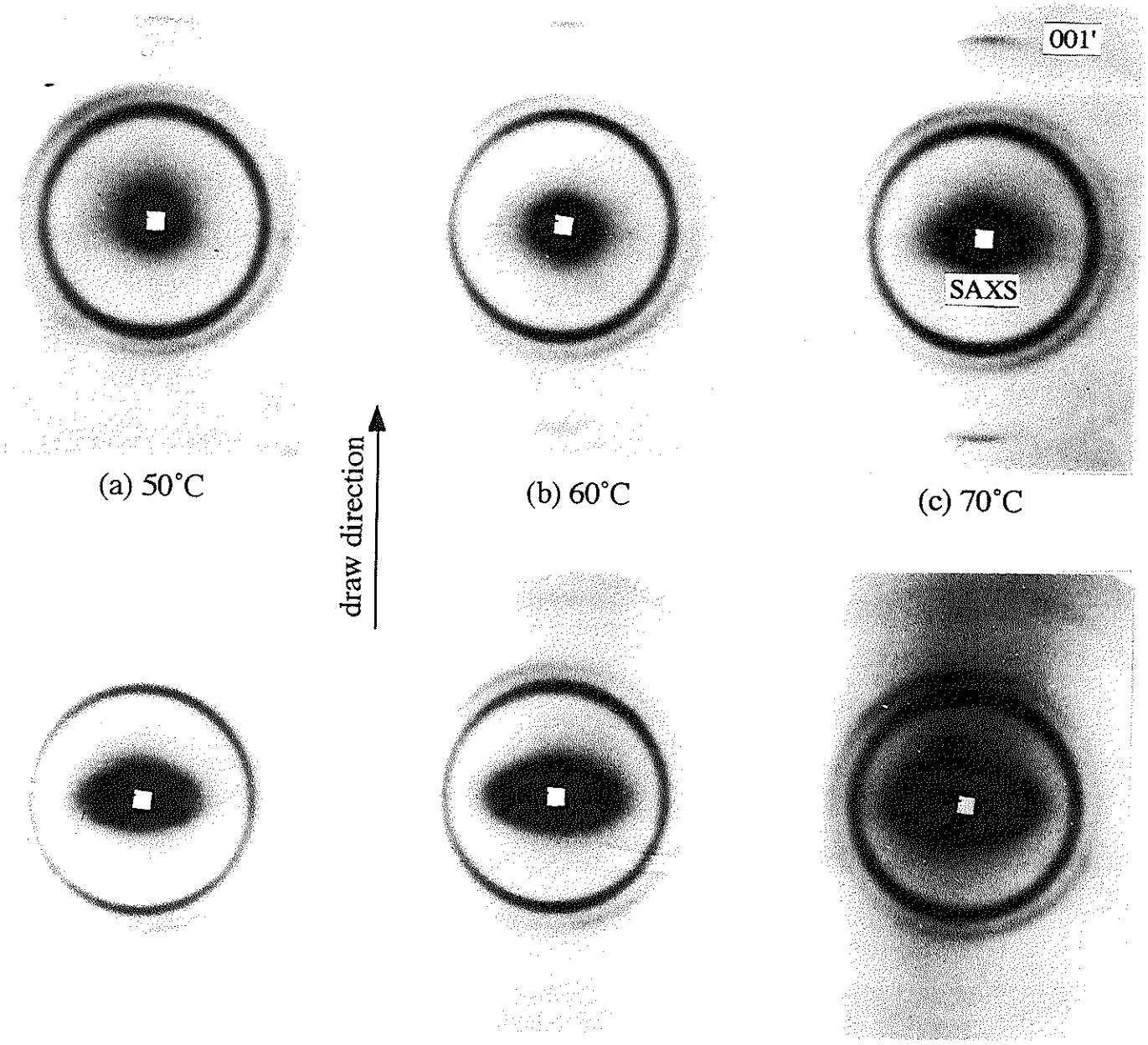

Fig. 6

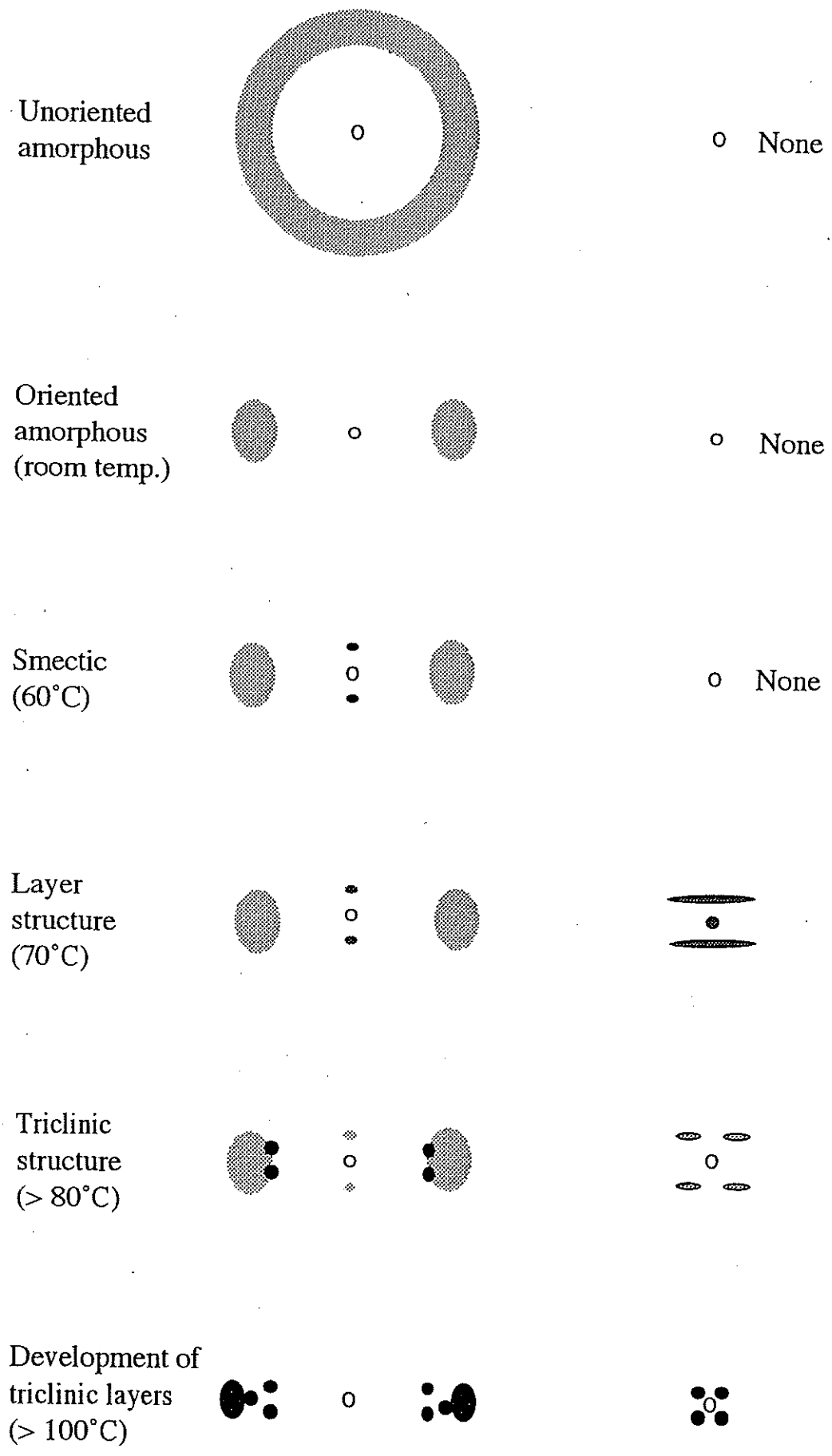
WAXS
SAXS
Unoriented amorphous
None
Oriented amorphous (room temp.)
None
Smectic (60°C)
None
Layer structure (70°C)
Triclinic structure (> 80°C)
Development of triclinic layers (> 100°C)

Fig. 7

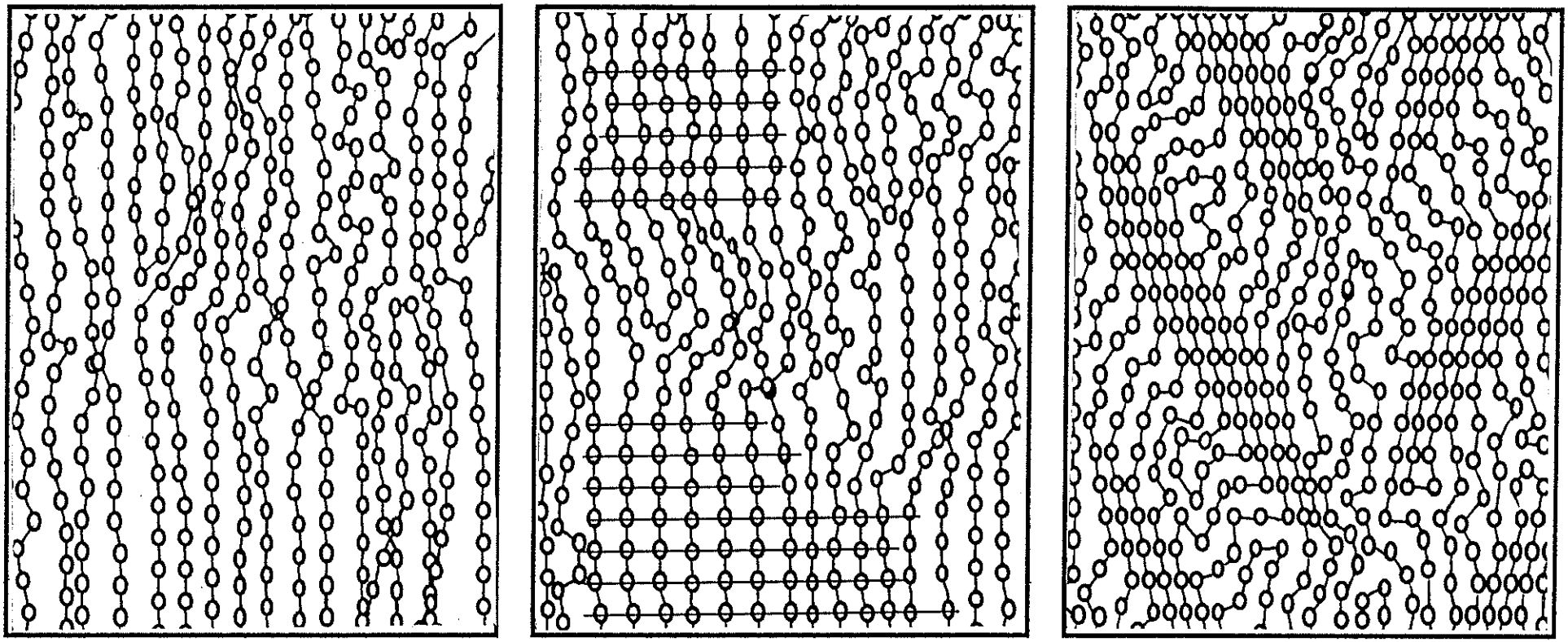

(a) nematic (b) smectic (c) triclinic

Fig. 8

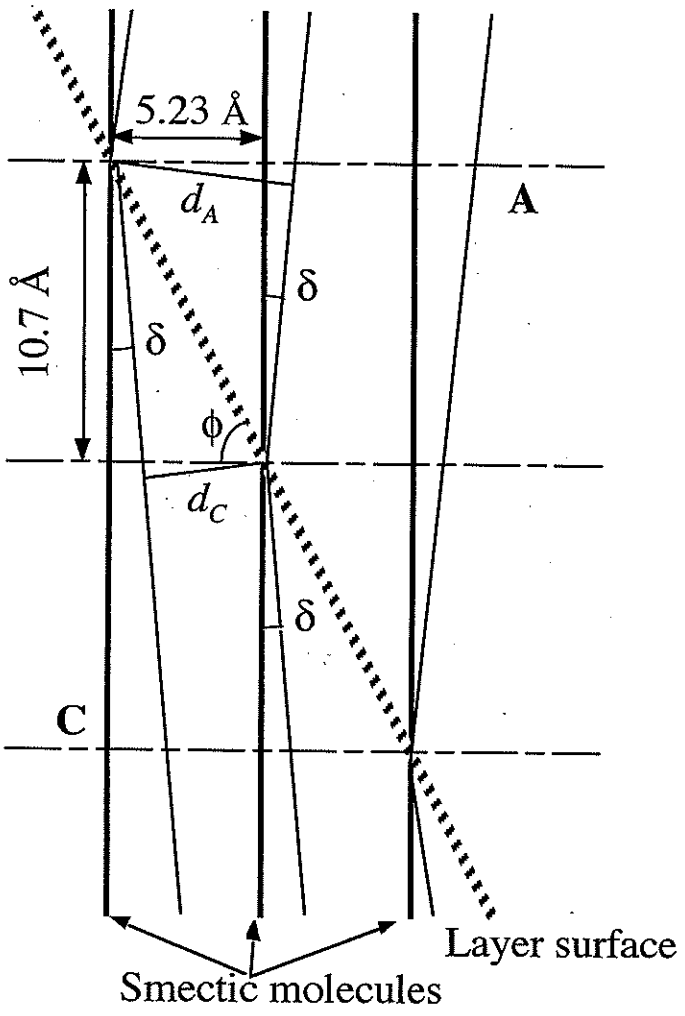
5.23 Å
10.7 Å
d_A
A
δ
δ
ϕ
d_C
δ
C
Layer surface
Smectic molecules

(a)

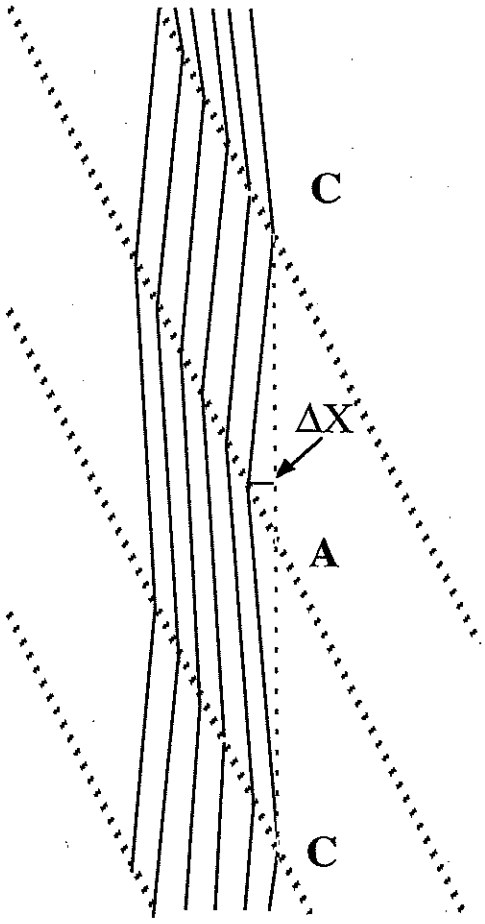
C
ΔX
A
C

(b)

Fig. 9

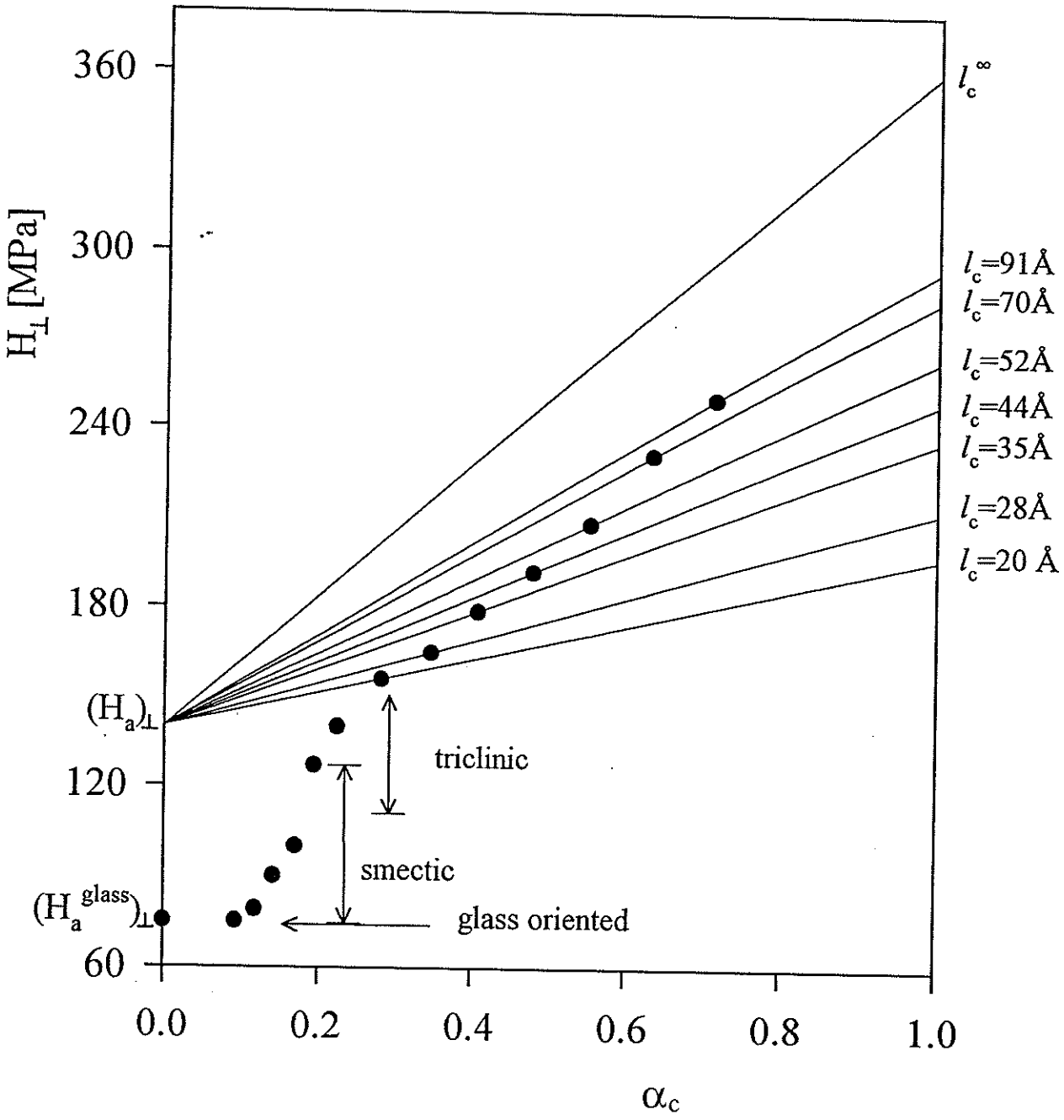
360
300
240
180
120
60
$H_\perp$ [MPa]
$(H_a)_\perp$
$(H_a^{glass})_\perp$
l_c^∞
l_c=91Å
l_c=70Å
l_c=52Å
l_c=44Å
l_c=35Å
l_c=28Å
l_c=20 Å
triclinic
smectic
glass oriented
0.0
0.2
0.4
0.6
0.8
1.0
α_c

Fig. 10

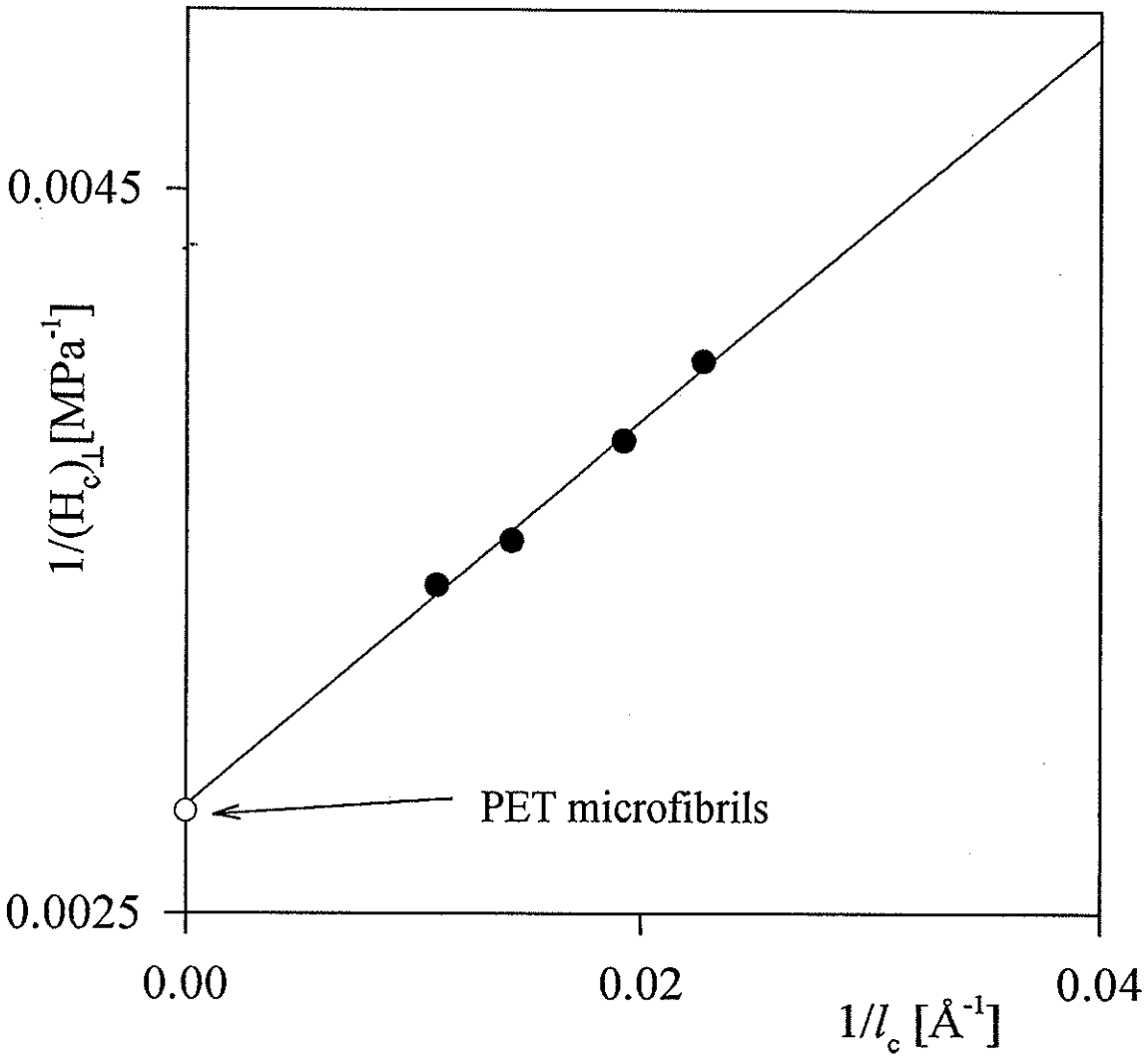
0.0045
0.0025
$1/(H_c)_\perp$ [MPa^{-1}]
PET microfibrils
0.00
0.02
0.04
$1/l_c$ [Å^{-1}]

Fig. 11